Journal of ELECTRONIC MATERIALS, Vol. 46, No. 7, 2017
DOI: 10.1007/s11664-017-5458-0

Synthesis, Characterization, and Photocatalytic Behavior of Praseodymium Carbonate and Oxide Nanoparticles Obtained by Optimized Precipitation and Thermal Decomposition

SEIED MAHDI POURMORTAZAVI,[1,7] MEHDI RAHIMI-NASRABADI,[2,3,8] MUSTAFA AGHAZADEH,[4] MOHAMMAD REZA GANJALI,[5,6] MEISAM SADEGHPOUR KARIMI,[5] and PARVIZ NOROUZI[5,6]

1.—Faculty of Material and Manufacturing Technologies, Malek Ashtar University of Technology, P.O. Box 16765-3454, Tehran, Iran. 2.—Faculty of Pharmacy, Baqiyatallah University of Medical Sciences, Tehran, Iran. 3.—Department of Chemistry, Imam Hossein University, Tehran, Iran. 4.—Nuclear Science and Technology Research Institute (NSTRI), P.O. Box 14395-834, Tehran, Iran. 5.—Center of Excellence in Electrochemistry, University of Tehran, Tehran, Iran. 6.—Biosensor Research Center, Endocrinology and Metabolism Molecular-Cellular Sciences Institute, Tehran University of Medical Sciences, Tehran, Iran. 7.—e-mail: pourmortazavi@yahoo.com. 8.—e-mail: rahiminasrabadi@gmail.com

Direct precipitation of insoluble praseodymium carbonate salt by reaction of the corresponding cation and anion was utilized in this study. This facile, routine, and effective route was optimized statistically through an orthogonal array design for fabrication of nanoparticles, using a Taguchi method to quantitatively evaluate the effects of the major operation conditions on the particle diameter via analysis of variance. The results indicated that high-purity particles with very small dimension (30 nm) could be produced simply by regulating the cation and anion concentrations and flow rate of introducing the cation into the anion solution. The product was thermally decomposed to yield praseodymium oxide nanoparticles by single-stage reaction. Both products were characterized using various conventional techniques including x-ray diffraction analysis, scanning electron microscopy, transmission electron microscopy, Fourier-transform infrared spectroscopy, and ultraviolet–visible diffuse reflectance spectroscopy to monitor the effects of the optimization on their physicochemical properties. Furthermore, the photocatalytic behavior of the nanoparticles was evaluated for treatment of water polluted with methyl orange, revealing high efficiency for degradation of the organic pollutant.

Key words: Praseodymium carbonate, nanoparticles, photocatalyst, carbonation, direct precipitation, particle size control

INTRODUCTION

Regulated preparation of well-defined inorganic materials is an area of interest among material scientists worldwide, mostly due to their potential for application in varied fields.[1–4] Praseodymium oxides are critical ingredients of different catalytic systems, including those used in combustion reactions, oxygen storage components, as well as materials with higher electrical conductivity.[5–7] Wang and coworkers reported synthesis of single-crystalline Pr_6O_{11} nanotubes by a molten salt method at 840°C using bulk Pr_6O_{11} and NaCl or KCl.[8] Hydrothermal synthesis of $Pr(OH)_3$ nanorods was reported by Huang and his team. The reaction was reported to be performed at 180°C, and the product was further calcinated to yield Pr_6O_{11} nanorods.[9]

(Received August 30, 2016; accepted March 16, 2017; published online March 28, 2017)

Crystalline praseodymium oxide (PrO_x) has shown good potential for application in nano- and microelectronic devices as this compound offers high effective dielectric constant and negligible leakage current.[10] It has also been used in highly conductive materials,[11] as a semiconducting oxide for dielectric materials,[12] as well as in ethanol vapor sensors,[13] organic light-emitting diodes,[14] high-temperature pigments,[6] catalysts,[15,16] and nonvolatile ferroelectric random-access memory (Nv-FRAM) devices.[17] Moreover, praseodymium as a member of the lanthanides is capable of complex formation with Lewis bases (i.e., thiols, aldehydes, amines, etc.) via interaction of its *f*-orbital with the base functional group. Thus, lanthanide compounds may display attractive photocatalytic behavior for future applications in water treatment and pollution removal.

Common routes used for synthesis of praseodymium carbonate and oxide include thermal decomposition of precursor complex,[18] electrodeposition,[19] precipitation,[20] sol–gel techniques,[21] and the hydrothermal method,[9] but new, simple, rapid, and cheap methods for synthesis of nanoparticles of this element and its other family members are still required, especially with greater simplicity and milder operation conditions.

Consequently, in this work, we focused on synthesis of praseodymium carbonate (for later use as a precursor for preparation of praseodymium oxide nanoparticles by calcination) through an optimized yet simple, fast, and controllable direct precipitation method. Due to the importance of optimization of this route for successful synthesis, the Taguchi method, which is a frequently used combined mathematical and statistical technique, was applied. This method has proven to be very reasonable for characterization of multivariable processes, since it requires a smaller number of experiments for optimization of the parameters and can determine operating conditions with minimum effect on the outcome of the process.[22–25] The main aim of this work is to determine an optimized route for synthesis of praseodymium carbonate salt in the form of noncrystalline particles with minimal particle size distribution, as well as to evaluate the effects of the operating conditions on the dimension of the product. Previous studies have shown that the major operating conditions influencing the outcome of this reaction in terms of product characteristics include the concentrations of the cation and anion as well as the temperature and mixing flow rate,[9,21–28] hence we focused directly on application of an experimental design procedure to investigate the role of these four parameters. A further aim was to investigate the use of this product as a precursor for single-stage synthesis of praseodymium oxide nanoparticles via thermal decomposition. In the final stage of this work, methyl orange (MO) degradation was used as a probe reaction to assess the photocatalytic activity of the synthesized praseodymium carbonate and oxide nanoparticles.

EXPERIMENTAL PROCEDURES

Materials and Apparatus

Reagent-grade praseodymium nitrate and sodium carbonate and analytical-grade ethanol were used as received from Merck (Germany). Scanning electron micrographs of the samples were recorded using a Philips XL30 series instrument, applying gold film to make the surface of the samples conductive before loading into the instrument. The gold film was applied using a sputter coater (model SCD005; BAL-TEC, Switzerland). Transmission electron microscopy (TEM) images were obtained using a Zeiss model EM900 from samples coated on a Cu grid with a carbon layer. X-ray powder diffraction (XRD) analysis was conducted using a Rigaku D/Max 2500 V diffractometer with graphite monochromator and Cu target. Fourier-transform infrared (FT-IR) spectra were recorded using a Bruker Equinox 55 IR using KBr. For ultraviolet–visible (UV–Vis) measurements, praseodymium carbonate and oxide particles were dispersed in aqueous medium and studied in the range from 200 nm

Table I. Assignment of factors and levels in experiments using an OA_9 (3^4) matrix and mean width of praseodymium carbonate produced

Experiment number	Pr^{3+} concentration (M)	CO_3^{2-} concentration (M)	Pr^{3+} feed flow rate (ml/min)	Temperature (°C)	Diameter of praseodymium carbonate particles (nm)
1	0.01	0.01	2.5	0	36
2	0.01	0.05	10.0	30	30
3	0.01	0.25	40.0	60	39
4	0.05	0.01	10.0	60	36.5
5	0.05	0.05	40.0	0	37
6	0.05	0.25	2.5	30	42
7	0.25	0.01	40.0	30	47
8	0.25	0.05	2.5	60	44
9	0.25	0.25	10.0	0	46

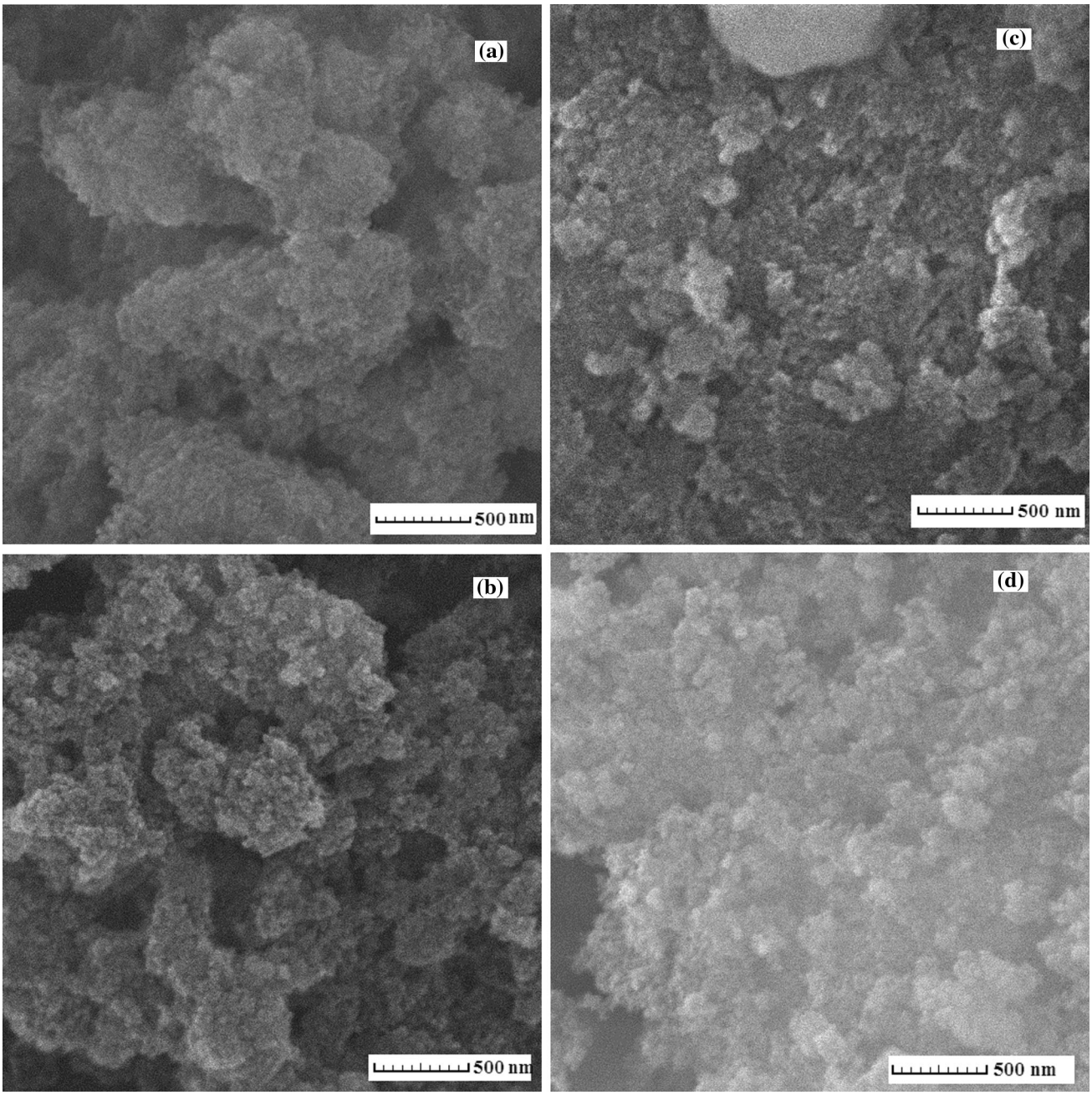

Fig. 1. SEM images of praseodymium carbonate nanoparticles obtained by direct precipitation method in different runs of the experimental design in Table I: (a) run 2, (b) run 4, (c) run 6, and (d) run 8.

to 700 nm using a PerkinElmer Lambda 35 UV–Vis spectrophotometer.

UV–Vis diffuse reflectance spectra (UV–Vis DRS) were obtained under ambient conditions using an AvaSpec-2048-TEC instrument. The concentration of the organic pollutant in the treated water samples was also studied by UV–Vis spectrometry using a PerkinElmer Lambda 25.

The samples were also studied by thermogravimetry and differential thermal analysis (TG/DTA) in the range from 30°C to 800°C using a Stanton Redcroft instrument (STA-780 series) with heating rate of 10°C/min under inert atmosphere (nitrogen blown at 50 mL/min).

Precipitation Reaction

Praseodymium carbonate particles were prepared by introduction of a flow of praseodymium nitrate solution of various concentrations at different rates into sodium carbonate solution under rapid stirring at various temperatures. After reaction completion, the product was filtered and washed with distilled water and ethanol, then dried in an oven at 80°C for

4 h. The variables considered for optimization in the Taguchi method were the concentrations of the praseodymium and carbonate solutions, the addition flow rate (F_z), and the temperature; an overview of the different levels of the parameters used and the resulting dimensions is presented in Table I.

Synthesis of Oxide Nanoparticles

Praseodymium oxides were prepared by subjecting the carbonate salt prepared under the optimal conditions to thermal decomposition in a furnace under static air atmosphere at 650°C for 4 h. The experiments were based on use of 0.25 g precursor loaded into the oven in a 40 mm × 20 mm alumina crucible, which was well wrapped using thin copper

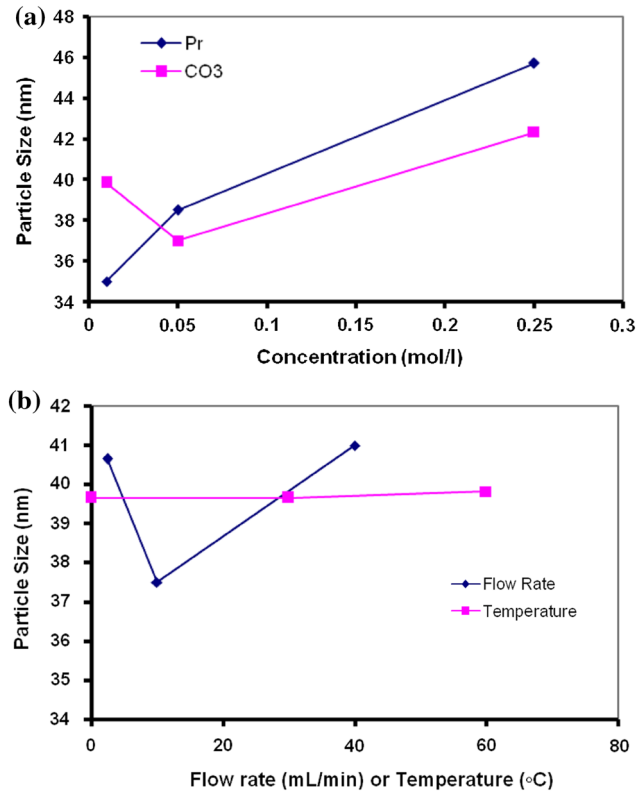

Fig. 2. Average effects of investigated variables at different levels on the diameter of the praseodymium carbonate nanoparticles. (a) Concentration of reagents and (b) flow rate and temperature.

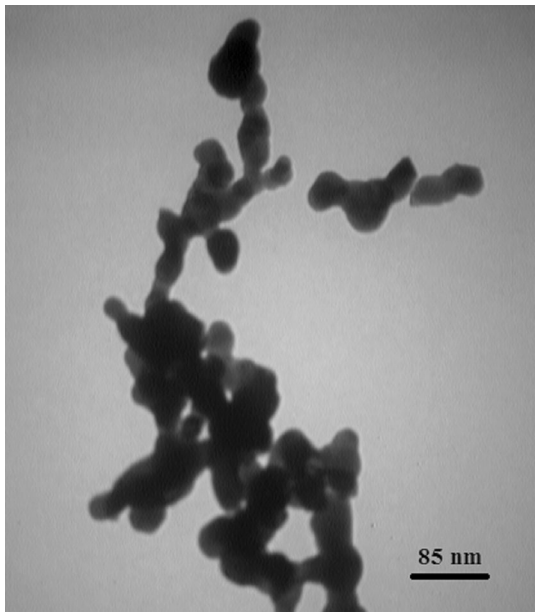

Fig. 3. TEM image of praseodymium carbonate nanoparticles precipitated under optimum conditions.

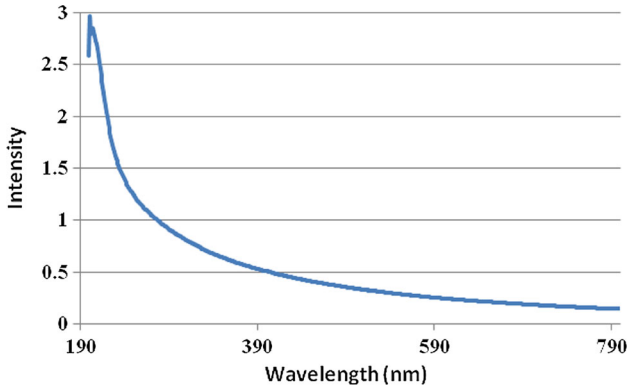

Fig. 4. FT-IR spectra of praseodymium carbonate nanoparticles precipitated under optimum conditions.

Table II. ANOVA table for synthesis of praseodymium carbonate particles using precipitation procedure by $OA_9(3^4)$ matrix with diameter of synthesized praseodymium carbonate particles (nm) as response

					Pooled[a]			
Factor	**Code**	**DOF**	**S**	**V**	**DOF**	**S′**	**F′**	**P′**
Praseodymium concentration (mol/L)	Cu	2	177.4	88.7	2	177.4	3175.8	73.1
Carbonate concentration (mol/L)	WO_4	2	42.7	21.4	2	42.7	764.8	17.6
Flow rate (mL/min)	F	2	22.4	11.2	2	22.4	400.8	9.2
Temperature (°C)	T	2	0.06	0.03	–	–	–	–
Error	E	–	–	–	2	0.06	–	0.1

[a]Significance was set at 90% confidence level; pooled error results from pooling insignificant effect.

foil to avoid sample loss; the reaction product was collected and used for further analyses.

Diffuse Reflectance Spectroscopy (DRS)

To study the optical bandgap energy (OBGE) of the prepared praseodymium carbonate and oxide nanostructures, UV–Vis DRS was used. The OBGE is defined as the lowest photon energy required to excite an electron from the valence band of a semiconductor to its conduction band. The relationship between the absorption edge of a semiconductor and energy is expressed by the following equation[29]:

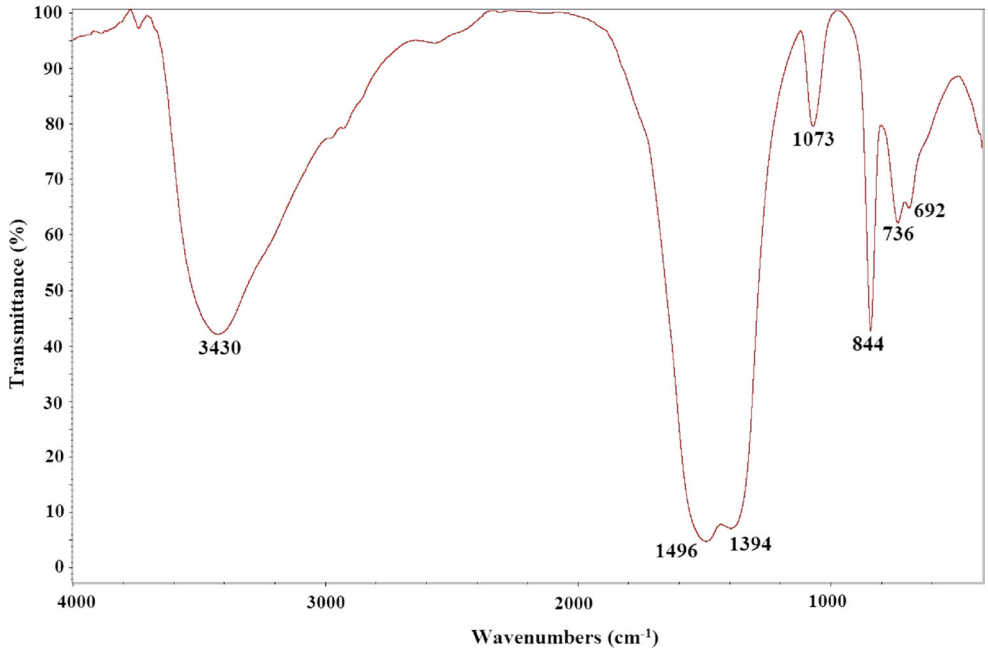

Fig. 5. UV–Vis absorption spectrum of praseodymium carbonate nanoparticles (precipitated under optimum conditions) dispersed in ethanol.

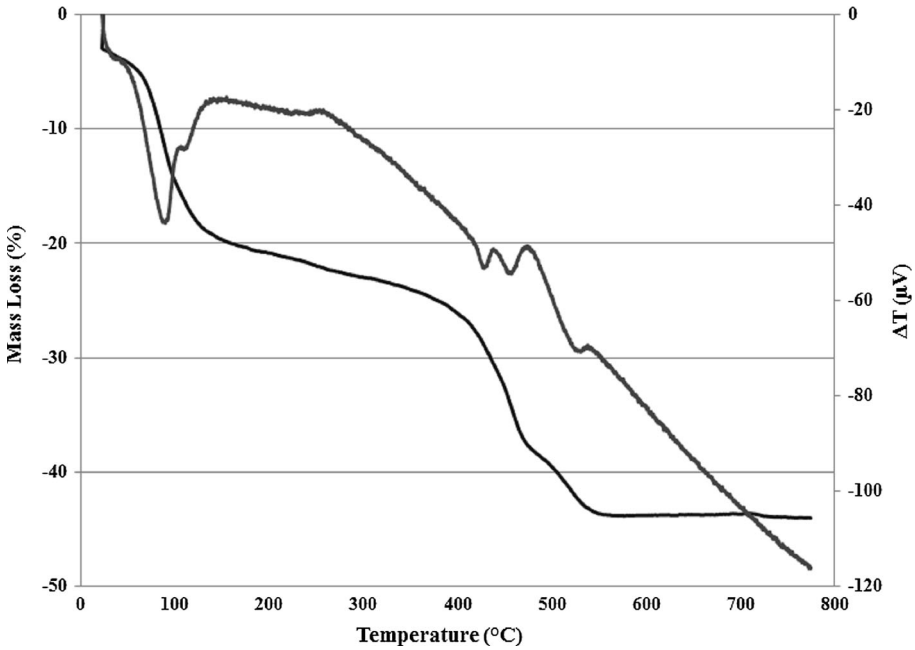

Fig. 6. TG and DTA curves for praseodymium carbonate nanoparticles prepared by precipitation method under optimum conditions (sample weight 5.0 mg, heating rate 10°C/min, nitrogen atmosphere).

$$\alpha h\upsilon = A\left(h\upsilon - E_g\right)^{\eta}, \quad (1)$$

known as Tauc's equation, where h, υ, α, and E_g refer to Planck's constant, the frequency of light, the absorption coefficient, and the OBGE. A and η are constant values. η can be either $\frac{1}{2}$ or 2 depending on whether the transition mechanism is direct (as is the case of the present semiconductor) or indirect.

Photocatalytic Activity of Nanoparticles

The effect of the presence of praseodymium carbonate and oxide nanoparticles as catalysts in the photodegradation of methyl orange (MO) in aqueous medium under UV irradiation was studied. For these studies, a high-pressure Hg lamp (250 W, $\lambda > 254$ nm) was fixed concentrically inside a Pyrex double-pipe air-lift used as a photoreactor.

Experiments were performed by adding 0.05 g photocatalytic nanoparticles to 500 mL 5 mg/L aqueous MO solution and stirring the resulting mixture for 20 min before applying UV irradiation. The reactor temperature was kept at 25°C. Before the beginning of the reaction and also at 10-min intervals from its start (i.e., at 10 min, 20 min, 30 min, 40 min, and 50 min after reaction onset), samples were taken from the reaction mixture and their MO content evaluated by UV–Vis spectrometry at the λ_{max} of MO.

Using the relationship between the concentration (C) and the absorbance of light (A) by a solution (Eq. 2, Beer–Lambert equation)[30]:

$$A = \varepsilon bC, \quad (2)$$

in which ε and b refer to the molar absorptivity and the path length of light through the solution, the absorbance values after time t [i.e., A_t corresponding to the concentration of the solution at time t (C_t)], and the initial absorbance of the solution (i.e., A_0 corresponding to the initial concentration C_0) were divided as shown in Eq. 3:

$$A/A_0 = C/C_0 \quad (3)$$

and the A_t and A_0 values used to calculate the photocatalytic degradation efficiency using Eq. 4:

$$\text{Degradation efficiency } (\%) = ((A_0 - A_t)/A_0) \times 100. \quad (4)$$

For the case of the kinetics of photocatalytic degradation of organic species at low initial concentration, the Langmuir–Hinshelwood model (Eq. 5) can be used[29,30]:

$$-\mathrm{d}C/\mathrm{d}t = k_{app} \times C, \quad (5)$$

where C, k_{app}, t, and $-\mathrm{d}C/\mathrm{d}t$ are the concentration of the organic species, rate constant, degradation time, and reaction rate, respectively.

RESULTS AND DISCUSSION

Optimization of Direct Precipitation Reaction by Statistical Experimental Design

Simply mixing the corresponding cation and anion to yield an insoluble salt is a common method for synthesis of such materials.[29,30] Fine-tuning of the product dimension is a rather sophisticated task requiring clear understanding of the interactions between the reagents but can be simplified by use of statistical approaches.

The factors summarized in Table I, chosen based on previous work,[9,21–28] were applied at different levels and the corresponding mean diameter of the resulting carbonate particles recorded. SEM images of several samples prepared under the conditions of Table I are shown in Fig. 1, to confirm these experimental results.

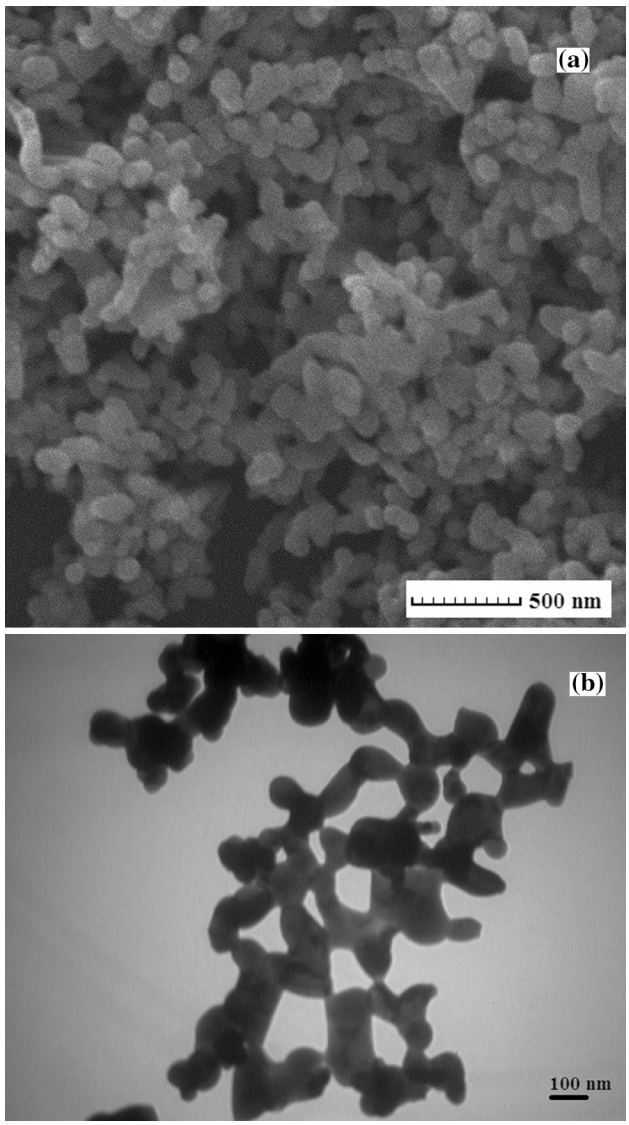

Fig. 7. (a) SEM and (b) TEM images of praseodymium oxide nanoparticles obtained via thermal decomposition of precursor.

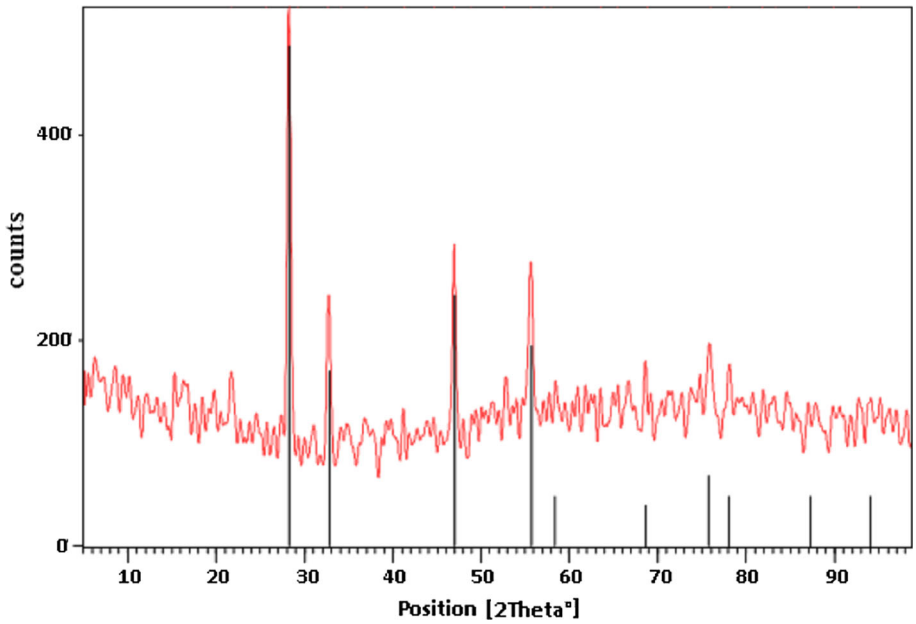

Fig. 8. XRD pattern of praseodymium oxide nanoparticles prepared by thermal decomposition of precursor.

Analysis of such data in the absence of interactions among the variables includes determination of the optimum conditions, identification of the influence of each factor on the outcome, and estimation of the result expected under the optimal conditions.

The average diameter of the praseodymium carbonate particles obtained using the different levels of the factors (Fig. 2) was calculated by averaging the diameter of the particles produced in the experiments in which one factor was at a given level; e.g., in the case of carbonate concentration of 0.01 M (level 1), the sum of the results of experiments 1, 4, and 7 was divided by 3. These average values reveal how the dimension of the particles varied upon alteration of each factor.

The analysis of variance (ANOVA) of the diameter of the praseodymium carbonate particles is presented in Table II. This analysis of the effect of the three levels of the concentrations of praseodymium and carbonate ions (i.e., 0.01 M, 0.05 M, and 0.25 M) on the characteristics of the product showed that both these parameters significantly influenced the diameter of the particles. Next, the influence of the addition flow rate (F_z) at the three levels of 2.5 mL/min, 10 mL/min, and 40 mL/min was studied, also being shown to be a significant variable determining the product dimension. A similar ANOVA analysis was performed to evaluate the effect of the reactor temperature at three levels of 0°C, 30°C, and 60°C, on the basis of which the reactor temperature was shown to be an insignificant variable in terms of influencing the product dimension. In general, it was therefore concluded that, except for the reactor temperature, all three of the other factors were significant in determining the product dimension at 90% confidence level.

The results obtained from the ANOVA (Table II) and the average effect of the different levels (Fig. 2) were used to identify the optimum values of the variables as carbonate and praseodymium concentration of 0.05 M and 0.01 M and F_z of 10 mL/min. The optimal diameter of the praseodymium carbonate particles (Y_{opt}), obtained under these optimal conditions, was calculated according to the following expression[31,32]:

$$Y_{opt} = \frac{T}{N} + \left(C_{Pr} - \frac{T}{N}\right) + \left(C_{CO3} - \frac{T}{N}\right) + \left(F_Z - \frac{T}{N}\right), \quad (6)$$

where T/N is the average diameter of the praseodymium carbonate particles and C_{Pr}, C_{CO3}, and F_z are the praseodymium and carbonate concentrations and the flow rate of adding the cation to the anion, respectively. The confidence interval (CI) of Y_{opt} was also calculated using the following expression[31,32]:

$$CI = \pm\sqrt{\frac{F_\alpha(f_1,f_2)V_e}{N_e}}, \quad (7)$$

where $F_\alpha(f_1,f_2)$ is the critical F-value based on the degrees of freedom of f_1 and f_2 (at confidence level of 90%), f_1 and f_2 are the degrees of freedom (DOF) for the mean (DOF_m = 1) and pooled error term, respectively, and N_e signifies the number of effective replications, as calculated from the following equation:

$$N_e = \frac{N_{exp}}{DOF_m + \sum DOF_i}, \quad (8)$$

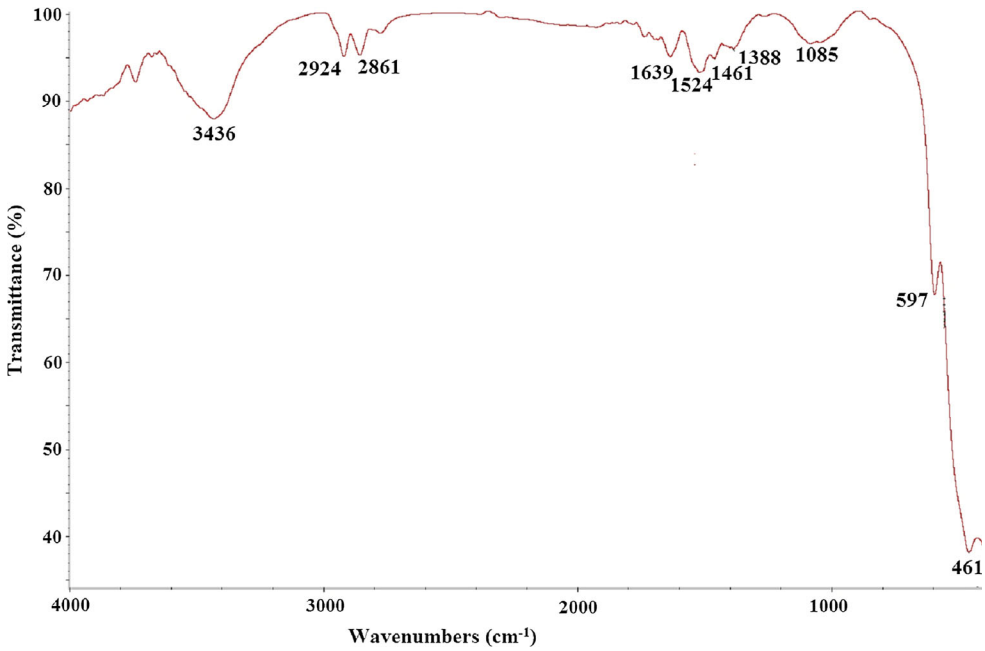

Fig. 9. FT-IR spectrum of praseodymium oxide nanoparticles after calcination of precursor at 650°C during 4 h.

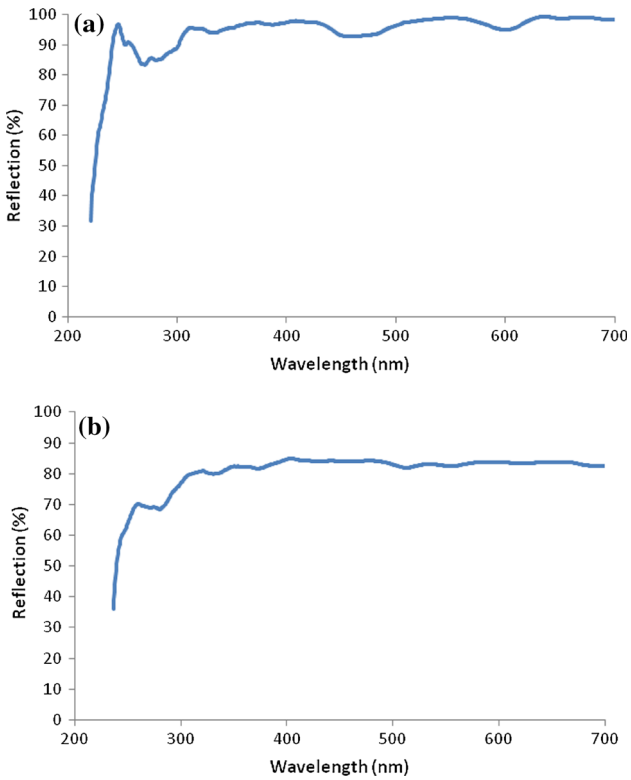

Fig. 10. Diffuse reflectance UV–Vis spectra of as-synthesized (a) praseodymium carbonate and (b) praseodymium oxide nanoparticles.

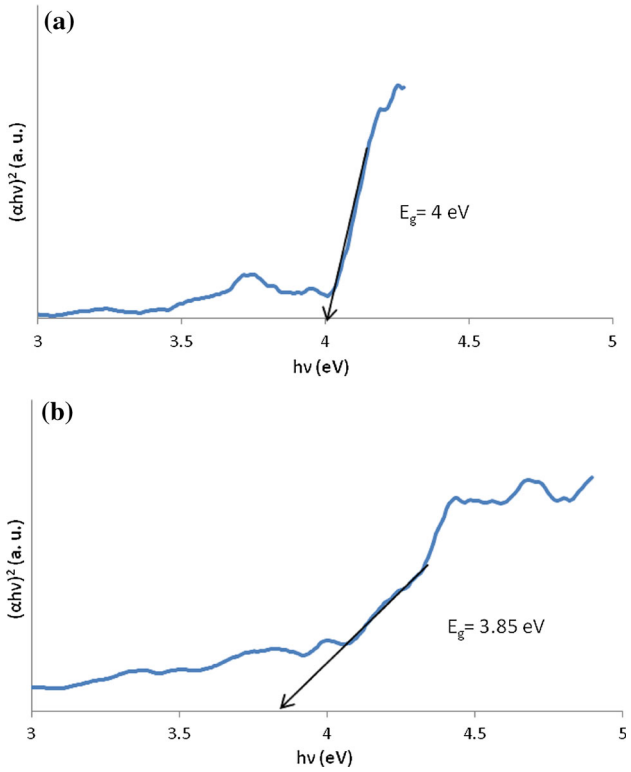

Fig. 11. Tauc plots for synthesized (a) praseodymium carbonate and (b) praseodymium oxide nanoparticles.

where N_{exp} is the number of experiments, DOF_m equals 1, and $\sum DOF_i$ is the sum of the degrees of freedom of the factors utilized in the prediction.

The calculations of Y_{opt} at confidence level of 90% led to Y_{opt} values of about 30 ± 0.5 nm. The SEM results revealed good agreement between these calculated results (run 2) and those of the

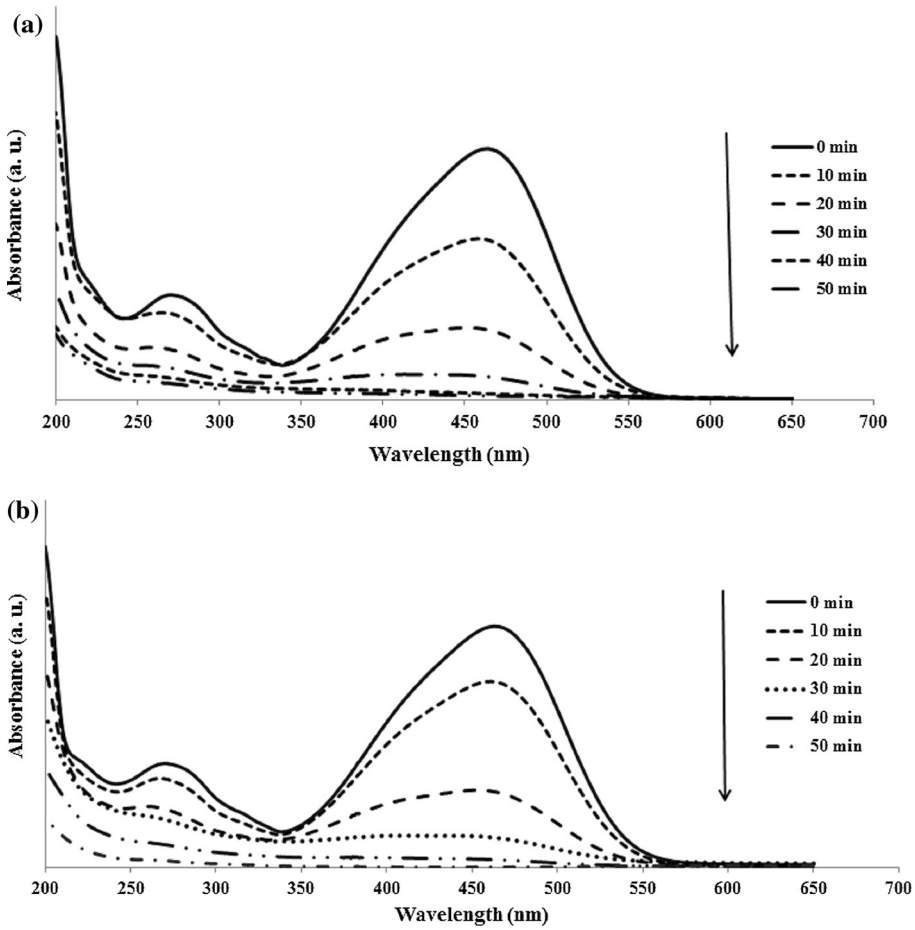

Fig. 12. MO UV–Vis absorbance spectra at different intervals for reaction mixtures containing 0.1 g/L of (a) praseodymium carbonate and (b) praseodymium oxide nanoparticles.

praseodymium carbonate nanoparticles prepared under the same conditions (about 30 nm) (Fig. 1a). To further check the accuracy of the calculations, the sample obtained using the optimal conditions was also investigated by TEM (Fig. 3), which not only confirmed the average diameter of about 30 nm, but also proved the nanoparticles to have spherical morphology. Samples prepared in this way (using the experimental conditions of run 2) were further characterized to evaluate their physical and chemical properties, and also utilized as precursor for synthesis of praseodymium oxide nanoparticles by thermal decomposition.

FT-IR, UV–Vis, and Thermal Analysis of Product

Optimally fabricated praseodymium carbonate nanoparticles were firstly explored by FT-IR spectroscopy; the results are presented in Fig. 4. The absorption bands of the vibrations of CO_3^{2-} were observed in the range of 400 cm^{-1} to 1800 cm^{-1}.[33,34] The strong and wide band with maximum at about 1397 cm^{-1} was attributed to asymmetric stretching vibrations of the anion, and that at 1513 cm^{-1} to the υ_3 mode of CO_3^{2-} group. Furthermore, the bands at 1079 cm^{-1}, 844 cm^{-1}, 747 cm^{-1}, and 699 cm^{-1} were assigned to stretching modes of carbonate.[35] Also, stretching and bending vibrations of O–H were detected at 3407 cm^{-1}, indicating presence of surface-adsorbed water molecules in the structure of the product.

Figure 5 presents the UV–Vis absorption spectrum of the produced nanoparticles in water, confirming their nanoscale dimension and the narrow distribution of the particle size with small standard deviation, as concluded from the narrow absorption band observed in the wavelength range centered at about 190 nm in this experiment. This further supports the idea that the optimized conditions presented herein can lead to formation of nanosized praseodymium carbonate particles with narrow size distribution.[22,23]

Since this compound can be used as a precursor for preparation of praseodymium oxide by thermal decomposition, its thermal behavior was also studied; the results are shown in Fig. 6. The TG–DTA curves of the praseodymium carbonate nanoparticles showed two mass loss phenomena in the tested range. A rather weak mass loss was observed from

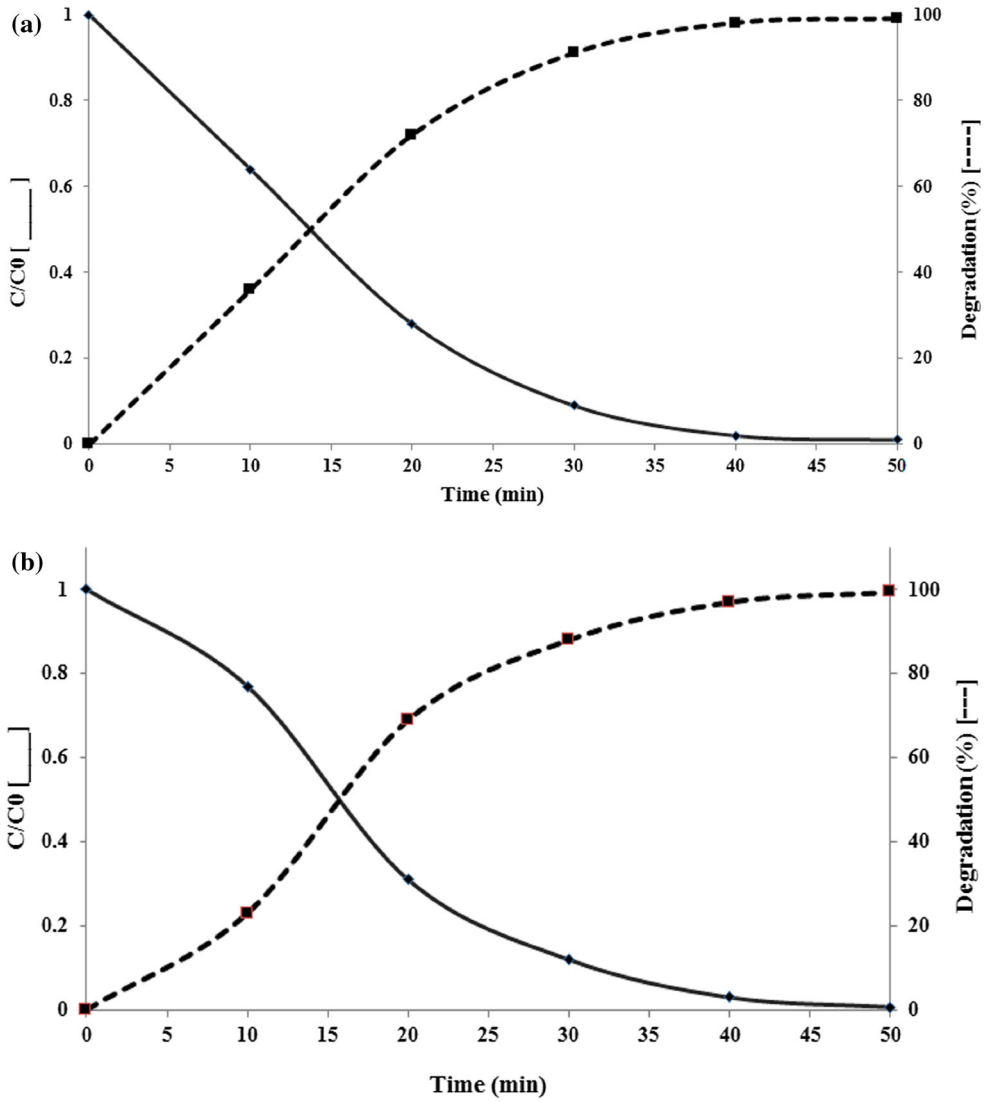

Fig. 13. Changes in C/C_0 and degradation of MO solution subjected to UV irradiation in presence of (a) praseodymium carbonate and (b) praseodymium oxide nanoparticles.

about 50°C to 250°C, and a second loss occurred from above 300°C up to 550°C. The overall mass loss in these two stages reached almost 43% of the sample mass. The first phenomenon in the range of 50°C to 250°C, which was responsible for around 20% mass loss, was ascribed to dehydration of water content of the sample, while the second, which caused a further 23% loss, was due to decomposition of the carbonate salt into the oxide of praseodymium. Since no further losses occurred above temperature of 550°C, it was decided that the thermal decomposition reaction was completed here, thus temperatures above this would be suitable for the decomposition stage.

Thermal Decomposition Reaction

Based on the initial information gained from the thermal analysis experiments, praseodymium oxide nanoparticles were fabricated by calcination of carbonate nanoparticles at 650°C for 4 h. The reaction was performed in air atmosphere due to the nature of the product. The obtained product was studied by SEM; the results are shown in Fig. 7, confirming that the oxide nanoparticles retained the spherical morphology of the precursor while their average size increased to a value of about 82 nm, as further confirmed by the TEM image of praseodymium oxide prepared under the optimum conditions in Fig. 7b.

The chemical properties of the product were then evaluated using XRD and FT-IR techniques. Figure 8 presents the XRD pattern of the produced oxide nanoparticles, where all the peaks are in good agreement with those indexed for cubic praseodymium oxide phase reported elsewhere [Joint Committee on Powder Diffraction Standards (JCPDS) 00-006-0329]. This indicates that the product was

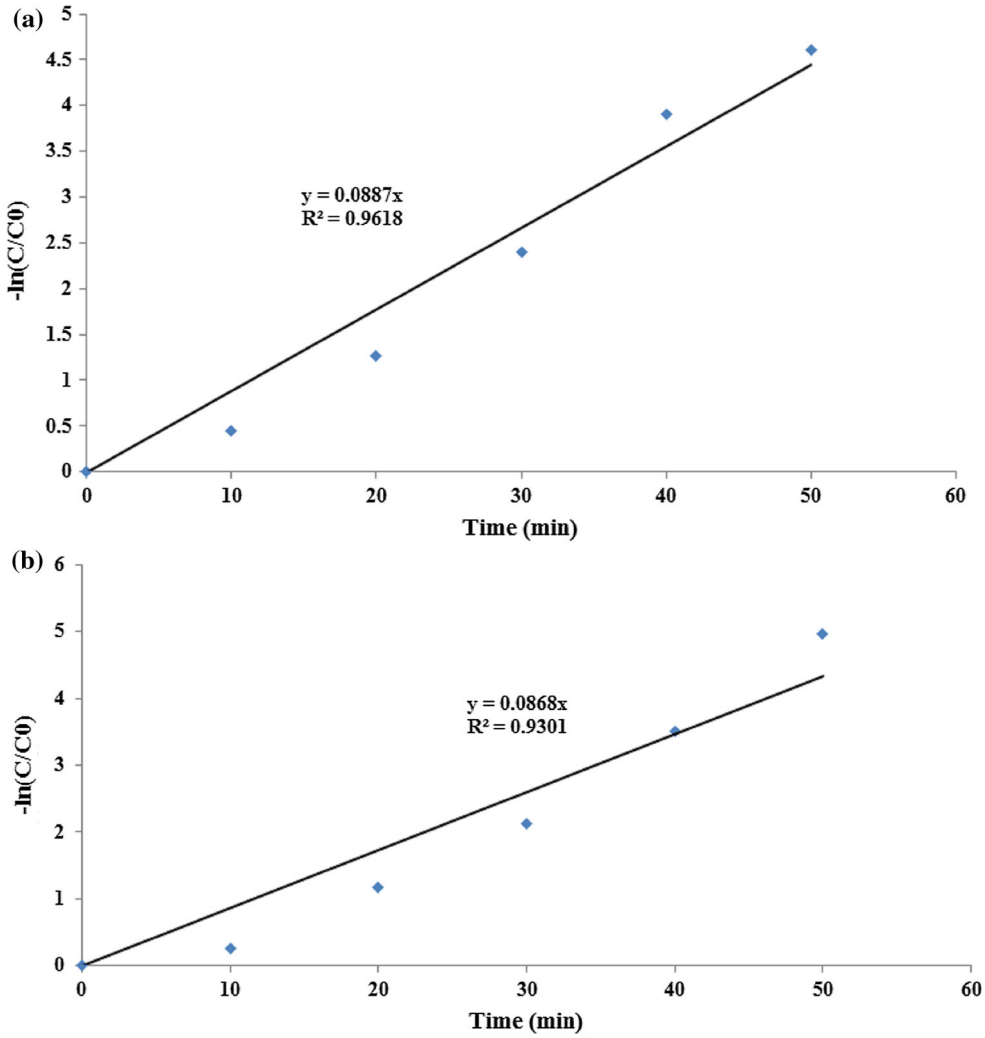

Fig. 14. $-\ln(C/C_0)$ versus irradiation time, indicating pseudo-first-order kinetics for MO degradation in presence of (a) praseodymium carbonate and (b) praseodymium oxide nanoparticles.

pure and had crystalline structure. The FT-IR spectrum of the sample (Fig. 9) prepared via thermal decomposition of the precursor at 650°C for 4 h was is very good agreement with literature results,[36–38] confirming the nature of the sample. In this figure, absorption bands corresponding to praseodymium oxide nanoparticles are observed at 596.77 cm^{-1} and 461.97 cm^{-1}. Comparing the FT-IR spectrum of this product with that of its precursor (Fig. 4), it is evident that the broad band at around 3434 cm^{-1}, which arises from stretching and bending vibrations of water molecules, is considerably reduced in Fig. 9.

DRS Studies

UV–Vis DRS results for the fabricated nanoparticles are shown in Fig. 10a and b, while Fig. 11a and b shows exemplary Tauc plots for these nanostructures. Based on these data, the OBGE for praseodymium carbonate and oxide was estimated to be around 4 eV and 3.85 eV, corresponding to absorption edges of around 310 nm and 322 nm, respectively.

Photodegradation Activity

Figure 12 presents the photocatalytic activity of the praseodymium carbonate and oxide nanoparticles. These data were acquired by monitoring the photodegradation performance of the catalysts by measuring the absorbance of light by the reaction solution. Furthermore, Fig. 13 shows the MO concentration versus time for reaction mixtures containing praseodymium carbonate and oxide nanoparticles, depicting the changes in C/C_0 versus UV irradiation time. These results clearly show that MO was effectively degraded in the presence of praseodymium carbonate and oxide nanoparticles, reaching maximum values of about 99% and 99.9% for after 50 min, respectively.

Photocatalytic decomposition of a single dye solution at low concentration followed pseudo-first-order

Table III. Pseudo-first-order reaction rate constant and conversion efficiency of praseodymium carbonate ($PrCO_3$) and praseodymium oxide (Pr_2O_3) nanoparticles after 50 min

	K (min^{-1})	Conversion (%)
Praseodymium carbonate	0.0887	99
Praseodymium oxide	0.1077	99.9

kinetics, being well approximated by the Langmuir–Hinshelwood (L–H) model, while without nanophotocatalyst and under similar conditions of continuous light irradiation, the concentration of the dye remained unaffected during the experimental period.[39–41] Plots of $-\ln(C/C_0)$ versus irradiation time for the studied nanoparticles are presented in Fig. 14a and b. The slopes of the linear regression obtained from these plots indeed indicate pseudo-first-order kinetics for the degradation of MO in the presence of praseodymium carbonate and oxide nanoparticles. The rate constants and maximum conversion values obtained for each catalyst are presented in Table III. These results clearly indicate that both praseodymium carbonate and oxide exhibited excellent photocatalytic effect for degradation of MO, leading to the expectation of similar effects on other organic pollutants.

CONCLUSIONS

The results presented herein show that the optimized direct precipitation method can be used as a very effective yet simple, fast, and controllable method for synthesis of praseodymium carbonate nanoparticles in aqueous medium. The product obtained using reaction conditions optimized by the Taguchi method was found to possess very good characteristics in terms of size, size distribution, morphology, and purity. The parameters investigated included the concentrations of praseodymium and carbonate solution, their addition flow rate, and the reactor temperature. All of the first three parameters were found to significantly influence the characteristics of the product at confidence level of 90%, while temperature did not. The product prepared using the optimal conditions had dimension of about 30 nm, in good agreement with the calculated diameter. This product was subjected to thermal decomposition to yield praseodymium oxide particles. SEM, TEM, XRD, UV–Vis, and FT-IR analyses confirmed the synthesis of pure praseodymium carbonate and oxide nanoparticles with limited size distribution in the two reactions. Finally, exploration of the photochemical behavior of the fabricated products revealed that praseodymium carbonate and oxide nanoparticles could be effectively applied for elimination of the organic pollutant.

ACKNOWLEDGEMENTS

Financial support of this work by the Iran National Science Foundation (INSF) and University of Tehran is gratefully acknowledged.

REFERENCES

1. M. Rahimi-Nasrabadi, S.M. Pourmortazavi, Z. Rezvani, K. Adib, and M.R. Ganjali, *Mater. Manuf. Process.* 34, 30 (2015).
2. K. Adib, M. Rahimi-Nasrabadi, Z. Rezvani, S.M. Pourmortazavi, F. Ahmadi, H.R. Naderi, and M.R. Ganjali, *J. Mater. Sci. Mater. Electron.* 4541, 27 (2016).
3. M. Esmaili and A. Habibi-Yangjeh, *Phys. Status Solidi A* 2529, 206 (2009).
4. S. Ramezani, A. Ghazitabar, and S.K. Sadrnezhaad, *J. Iran. Chem. Soc.* 2069, 13 (2016).
5. M. Shamshi Hassan, M. Shaheer Akhtar, K.-B. Shim, and O.-B. Yang, *Nanoscale Res. Lett.* 735, 5 (2010).
6. P. Šulcova, *J. Therm. Anal. Calorim.* 51, 82 (2005).
7. W. Wang, P. Lin, Y. Fu, and G. Cao, *Catal. Lett.* 19, 82 (2002).
8. X. Wang, J. Zhuang, and Y.D. Li, *Eur. J. Inorg. Chem.* 946, 5 (2004).
9. P.X. Huang, F. Wu, B.L. Zhu, G.R. Li, Y.L. Wang, X.P. Gao, H.Y. Zhu, T.Y. Yan, W.P. Huang, S.M. Zhang, and D.Y. Song, *J. Phys. Chem. B* 1614, 110 (2006).
10. H.J. Osten, J.P. Liu, P. Gaworzewski, E. Bugiel, P. Zaumseil, *IEEE IEDM Tech. Dig.* (2000), pp. 653–656.
11. S. Shrestha, C.M.Y. Yeung, C. Nunnerley, and S.C. Tsang, *Sens. Actuators A* 191, 136 (2007).
12. H.J. Mussig, J. Dabrowski, K. Ignatovich, J.P. Liu, V. Zavodin-sky, and H.J. Osten, *Surf. Sci.* 159, 504 (2002).
13. S.C. Tsang and C. Bulpitt, *Sens. Actuators B* 226, 52 (1998).
14. C.F. Qiu, H.Y. Chen, Z.L. Xie, M. Wong, and H.S. Kwok, *Appl. Phys. Lett.* 3485, 80 (2002).
15. K. Asami, K.-I. Kusakabe, N. Ashi, and Y. Ohtsuka, *Appl. Catal. A* 43, 156 (1997).
16. S. Bernal, F.J. Botana, G. Cifredo, J.J. Calvino, A. Jobacho, and J.M. Rodriguez-Izquierdo, *J. Alloys Compd.* 180, 271 (1992).
17. U. Chon, J.S. Shim, and H.M. Jang, *J. Appl. Phys.* 4769, 93 (2003).
18. M. Popa and M. Kakihana, *Solid State Ionics* 265, 141–142 (2001).
19. M. Shamshi Hassan, Y.-S. Kang, B.-S. Kim, I.-S. Kim, H.-Y. Kim, and M.-S. Khil, *Superlattices Microstruct.* 50, 139–144 (2011).
20. M. Shamshi Hassan, M. Shaheer Akhtar, K.-B. Shim, and O.-B. Yang, *Nanoscale Res. Lett.* 735, 5 (2010).
21. Y. Borchert, P. Sonström, M. Wilhelm, H. Borchert, and M. Bäumer, *J. Phys. Chem. C* 3054, 112 (2008).
22. M. Rahimi-Nasrabadi, S.M. Pourmortazavi, M.R. Ganjali, A.R. Banan, and F. Ahmadi, *J. Mol. Struct.* 85, 1074 (2014).
23. R.K. Roy, *A Primer on the Taguchi Method* (New York: Van Nostrand Reinhold, 1990).
24. M. Rahimi-Nasrabadi, S.M. Pourmortazavi, M.R. Ganjali, S.S. Hajimirsadeghi, and M.M. Zahedi, *J. Mol. Struct.* 31, 1047 (2013).
25. M. Rahimi-Nasrabadi, S.M. Pourmortazavi, A.A. Davoudi-Dehaghani, S.S. Hajimirsadeghi, and M.M. Zahedi, *CrystEngComm* 4077, 15 (2013).
26. M. Rahimi-Nasrabadi, S.M. Pourmortazavi, M. Khalilian-Shalamzari, S.S. Hajimirsadeghi, and M.M. Zahedi, *Cent. Eur. J. Chem.* 1393, 11 (2013).
27. S.M. Pourmortazavi, M. Rahimi-Nasrabadi, M. Khalilian-Shalamzari, H.R. Ghaeni, and S.S. Hajimirsadeghi, *J. Inorg. Organomet. Polym. Mater.* 333, 24 (2014).
28. S.M. Pourmortazavi, M. Rahimi-Nasrabadi, and S.S. Hajimirsadeghi, *J. Disper. Sci. Technol.* 254, 33 (2012).

29. Y. Fazli, S.M. Pourmortazavi, I. Kohsari, M. Sadeghpour Karimi, and M. Tajdari, *J. Mater. Sci. Mater. Electron.* 7192, 27 (2016).
30. Y. Bayat, S.M. Pourmortazavi, H. Ahadi, and H. Iravani, *Chem. Eng. J.* 432, 230 (2013).
31. S.M. Pourmortazavi, M. Taghdiri, V. Makari, and M. Rahimi-Nasrabadi, *Spectrochim. Acta Mol. Biomol. Spectrosc.* 1249, 136 (2015).
32. P.J. Ross, *Taguchi Techniques for Quality Engineering* (New York: McGraw-Hill, 1988).
33. M. Shamsipur, S.M. Pourmortazavi, S.S. Hajimirsadeghi, and M. Roushani, *Colloids Surf. A* 35, 423 (2013).
34. M. Pirhashemi and A. Habibi-Yangjeh, *J. Colloid Interface Sci.* 103, 474 (2016).
35. G. Wang, H. Wang, J. Bai, Z. Ren, and J. Bai, *Chem. Eng. J.* 386, 214 (2013).
36. X. Shang, W. Lu, B. Yue, L. Zhang, J. Ni, Y. Lv, and Y. Feng, *Cryst. Growth Des.* 1415, 9 (2009).
37. B. Klingenberg and M.A. Vannice, *Chem. Mater.* 2755, 8 (1996).
38. M. Rahimi-Nasarabadi, F. Ahmadi, S. Hamdi, N. Eslami, K. Didehban, and M.R. Ganjali, *J. Mol. Liq.* 216, 814 (2016).
39. T. Yu, X. Tan, L. Zhao, Y. Yin, P. Chen, and J. Wei, *Chem. Eng. J.* 86, 157 (2010).
40. G.K. Castello, *Handbook of Photocatalysts: Preparation, Structure and Applications* (New York: Nova Science, 2010).
41. M. Farbod and M. Kajbafvala, *Powder Tech.* 434, 239 (2013).